Oncogene KRAS activates fatty acid synthase, resulting in specific ERK and lipid signatures associated with lung adenocarcinoma

Arvin M. Gouw[a,b], Livia S. Eberlin[c,d], Katherine Margulis[c], Delaney K. Sullivan[a,b], Georgia G. Toal[a,b], Ling Tong[a,b], Richard N. Zare[c,1], and Dean W. Felsher[a,b,1]

[a]Division of Oncology, Department of Medicine, Stanford University School of Medicine, Stanford, CA 94305; [b]Division of Oncology, Department of Pathology, Stanford University School of Medicine, Stanford, CA 94305; [c]Department of Chemistry, Stanford University, Stanford, CA 94305; and [d]Department of Chemistry, The University of Texas at Austin, Austin, TX 78712

Contributed by Richard N. Zare, February 7, 2017 (sent for review October 27, 2016; reviewed by David C. Muddiman and Almut Schulze)

KRAS gene mutation causes lung adenocarcinoma. KRAS activation has been associated with altered glucose and glutamine metabolism. Here, we show that KRAS activates lipogenesis, and this activation results in distinct proteomic and lipid signatures. By gene expression analysis, KRAS is shown to be associated with a lipogenesis gene signature and specific induction of fatty acid synthase (FASN). Through desorption electrospray ionization MS imaging (DESI-MSI), specific changes in lipogenesis and specific lipids are identified. By the nanoimmunoassay (NIA), KRAS is found to activate the protein ERK2, whereas ERK1 activation is found in non–KRAS-associated human lung tumors. The inhibition of FASN by cerulenin, a small molecule antibiotic, blocked cellular proliferation of KRAS-associated lung cancer cells. Hence, KRAS is associated with activation of ERK2, induction of FASN, and promotion of lipogenesis. FASN may be a unique target for KRAS-associated lung adenocarcinoma remediation.

lipogenesis | lung | KRAS | MS | fatty acid synthase

Oncogene KRAS is a member of the RAS gene subfamily that is commonly mutated in human cancer, including lung adenocarcinoma (1, 2). The RAS genes encode membrane-localized G proteins that are components of several signaling cascades, including the Raf-MEK-ERK signal transduction pathway (2, 3). Most RAS mutations in cancer lead to constitutive activation of GTPase (2), resulting in cellular proliferation.

KRAS activation has been shown to alter glucose and glutamine metabolism (4). KRAS increases glycolytic flux, decreases oxidative TCA cycle flux, and promotes utilization of glutamine for anabolic pathways (4). In human pancreatic ductal adenocarcinoma (PDAC) cells, KRAS inhibits glutamate dehydrogenase that converts glutamine-derived glutamate into α-ketoglutarate to fuel the TCA cycle. KRAS also increases expression of GOT1, which converts glutamine-derived aspartate into oxaloacetate in a pathway that generates NADPH (5, 6). The shift from using glutamine to fuel the TCA cycle to using glutamine in a noncanonical NADPH-generating pathway is essential for the growth of PDAC cells. This metabolic change results in an increased NADPH/$NADP^+$ ratio maintaining redox balance. Changes in metabolism caused by KRAS are thought to play an essential role in the proliferation and survival of cancer (5, 7, 8). Before this study, the regulation of lipogenesis in lung adenocarcinoma by KRAS has not been established.

MS imaging (MSI), a spatially resolved label-free imaging technique, presents an attractive way to visualize the distribution of numerous known and unknown molecular ion species within a tissue of interest without molecule preidentification. MSI has been extensively investigated as a tool that enables delineation of cancerous tissues from their normal counterparts and categorizes various tumors. Several MSI methods have been used to delineate and categorize lung neoplasia. MALDI imaging on tissue microarrays was recently proposed for histopathological subtyping of nonsmall cell lung cancer into adenocarcinoma and squamous cell carcinoma (9). Airflow-assisted desorption electrospray ionization MSI was recently used to molecularly visualize postoperative human lung cancer specimens (10). In this study, we used desorption electrospray ionization MS imaging (DESI-MSI) for analyzing KRAS-driven metabolism in lung. DESI-MSI is an established, powerful technique for real-time in situ analysis of tissue metabolism (11–13). Tissue sections are bombarded with charged microdroplets containing a 1:1 mixture of dimethylformamide and acetonitrile, which are generated by electrospray, causing lipids and metabolites in the tissue samples to be dissolved and extracted. The continuous impact of the spray on the sample then creates a splash of secondary microdroplets containing dissolved analytes, which are captured by a mass spectrometer. A 2D chemical map of the tissue section can then be created based on MS analysis. DESI-MSI has been extensively used to interrogate the lipid profiles of lymphomas (14), renal cell carcinoma (15), thyroid cancer (16), pancreatic cancer (17), breast cancer (18), brain cancer (19), and other cancerous tissues (13, 20).

Here, we combined gene expression analysis, nanoscale proteomics, and MSI assays to investigate the relationship between KRAS mutations and lipid signatures in lung cancers. Nanoimmunoassay (NIA) analyses on human patient samples were used to examine KRAS vs. non-KRAS lung adenocarcinoma to show that KRAS is associated with phospho-ERK2 induction. Gene expression analyses and DESI-MSI of a murine KRAS lung model show that KRAS induces several genes involved in lipogenesis: sterol regulatory

Significance

We studied lung tumors induced by oncogene KRAS gene mutation using transgenic mice and human lung specimens. Gene expression analyses show that KRAS induces fatty acid synthase (FASN), promoting lipogenesis. Through desorption electrospray ionization MS imaging, we found specific lipid modifications in KRAS lung adenocarcinoma. Nanoimmunoassay identified specific KRAS-associated phosphoprotein signatures. We showed that KRAS activates the ERK2 protein, whereas non-KRAS lung adenocarcinoma shows elevated ERK1. We inhibited FASN by a small molecule, cerulenin, and this inhibition blocked cellular proliferation of KRAS-driven lung cancer cells. FASN inhibitors may, thus, present promising therapeutic agents for the treatment of KRAS-associated lung adenocarcinoma.

Author contributions: A.M.G., L.S.E., K.M., R.N.Z., and D.W.F. designed research; A.M.G., L.S.E., K.M., D.K.S., G.G.T., and L.T. performed research; A.M.G. and L.T. contributed new reagents/analytic tools; A.M.G., L.S.E., K.M., D.K.S., G.G.T., and D.W.F. analyzed data; and A.M.G., L.S.E., K.M., D.K.S., R.N.Z., and D.W.F. wrote the paper.

Reviewers: D.C.M., North Carolina State University; and A.S., Theodor Boveri Institute.

Conflict of interest statement: The material in this manuscript is the subject of a provisional application to the United States Patent and Trademark Office.

[1]To whom correspondence may be addressed. Email: zare@stanford.edu or dfelsher@stanford.edu.

This article contains supporting information online at www.pnas.org/lookup/suppl/doi:10.1073/pnas.1617709114/-/DCSupplemental.

binding protein (SREBP1), fatty acid synthase (FASN), and stearoyl CoA desaturase (SCD). Because the major regulatory site for fatty acid (FA) synthesis is on FASN, we decided to inhibit FASN along with others that have shown efficacy in inhibiting FASN in Nonsmall Cell Lung Cancer cells (21, 22). Notably, our results show that blocking FASN with a therapeutic agent prevents KRAS-associated lung cancer cells from proliferating. Thus, blocking FASN could represent a therapeutic route for treating KRAS-induced lung cancer.

Results

KRAS Induces Lipogenesis in Mouse and Human Lung Adenocarcinoma. The Tet system was used to conditionally express a mutant KRAS gene in mouse lung epithelium resulting in lung adenocarcinoma (23). We examined 13 metabolic pathways that were identified by 169 microarray probes (Table S1), and the results are plotted in the heat map (Fig. 1*A*). Gene expression analysis of these tumors showed increased expression of many metabolic genes. We found that a majority of the genes in the FA synthesis pathway were in the top 15 most differentially expressed genes (Fig. 1*B*). Among the lipogenesis genes shown to be induced, we note three particularly important genes. FASN is the regulatory site of FA synthesis (24), and SCD is the last enzyme in the pathway (25) (Fig. 1*C*). SREBP is the transcription factor that induces genes involved in FA, mevalonate, and cholesterol syntheses (26, 27). Induction of FASN, SCD, and SREBP was confirmed by quantitative PCR (qPCR) (Fig. 1*C*). Thus, KRAS induces lipogenesis pathways in murine lung adenocarcinoma.

Next, lipogenesis-associated genes were examined in human lung adenocarcinoma known to be KRAS-positive or -negative. Both KRAS-positive and -negative tumors overexpress lipogenesis genes (Fig. 2). This overexpression may reflect the necessity of FA synthesis in highly proliferating cells (28). SREBP is more elevated in KRAS-negative tumors, whereas SCD is more elevated in KRAS-positive tumors. FASN is highly up-regulated in both. Thus, induction of lipogenesis genes was observed in human KRAS-associated lung adenocarcinoma.

KRAS-Positive Vs. -Negative Tumors Exhibited Unique ERK Protein Signatures. KRAS activates ERK signaling (1, 3, 29). KRAS-positive vs. -negative lung tumors were found to exhibit ERK2 vs. ERK1 activation (Fig. 3 *A* and *B*). The KRAS-positive tumors exhibited increased pERK2a, pERK2b, and ERK2, and the KRAS-negative tumors exhibited increased ppERK1 and a decrease in the levels of ERK1 compared with matched normal lung tissue (Fig. 3 *C* and *D*). Using NIA, distinction between the different activation of various ERK phosphoisoforms by KRAS was achieved, which corroborates previous observations of ERK induction by KRAS (29, 30).

KRAS-Positive Tumors Exhibit Unique Lipid Profiles. DESI-MSI was performed on KRAS-positive mouse and human lung adenocarcinomas (Fig. S1). Tissues were harvested from transgenic mouse models harboring a conditional KRAS activation system (Fig. S2). We show representative mass spectra and selected 2D ion images from tissue samples of KRAS-induced lung adenocarcinoma and a tissue sample of control normal lung tissue (Fig. 4 and Fig. S3). As displayed in the 2D ion images of the KRAS-induced lung adenocarcinoma sample (Fig. 4*A*), high relative intensities of lipid ions were observed in specific regions of the cancer tissue section. Histopathologic evaluation of H&E-stained adjacent tissues sections confirmed that the high-lipid intensity regions strongly correlated with regions of accumulation of tumor cells (Fig. S3).

Differences in the DESI mass spectra extracted from these cancer regions were seen compared with spectra from normal lung tissues (Fig. 4*B*). For example, in the *m*/*z* region 700–1,000,

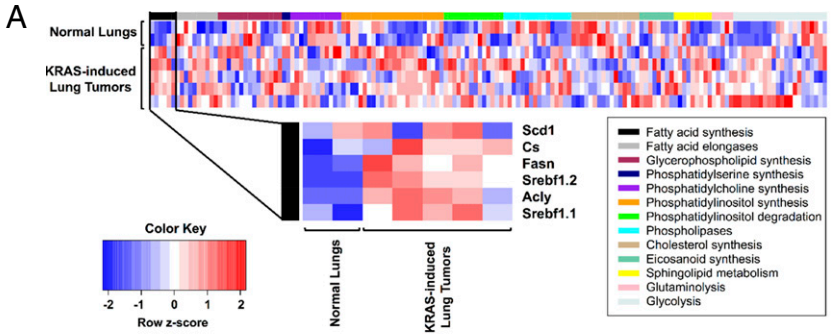

B

p-value	Gene	Pathway
0.000027	Sqle.1	Cholesterol synthesis
0.000128	Pgs1	Glycerophospholipid synthesis
0.000155	Cept1.1	Phosphatidylcholine synthesis
0.000176	Hk2	Glycolysis
0.000272	Gapdh	Glycolysis
0.000275	Lass6.2	Sphingolipid metabolism
0.000338	Pi4k2b.2	Phosphatidylinositol synthesis
0.000541	Pkm2	Glycolysis
0.001310	**Srebf1.2**	**Fatty acid synthesis**
0.002114	Lass2.1	Sphingolipid metabolism
0.002310	**Fasn**	**Fatty acid synthesis**
0.002599	**Acly**	**Fatty acid synthesis**
0.002949	Lass2.2	Sphingolipid metabolism
0.003001	Eno1	Glycolysis
0.003107	Aldoc	Glycolysis

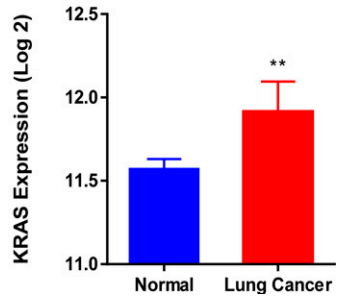

Fig. 1. Lipogenesis in KRAS-induced mouse lung cancer. (*A*) Microarray analysis showing up-regulation of FA synthesis genes in lung cancer. (*B*) The 15 most statistically significant genes differentially expressed between normal and KRAS-activated mouse lung tissue. Genes in bold are fatty acid synthesis genes. (*C*) Gene expression in normal ($n = 2$) and KRAS-activated mouse lung tissue ($n = 5$). **Statistical significance by *t* test for *P* value <0.01.

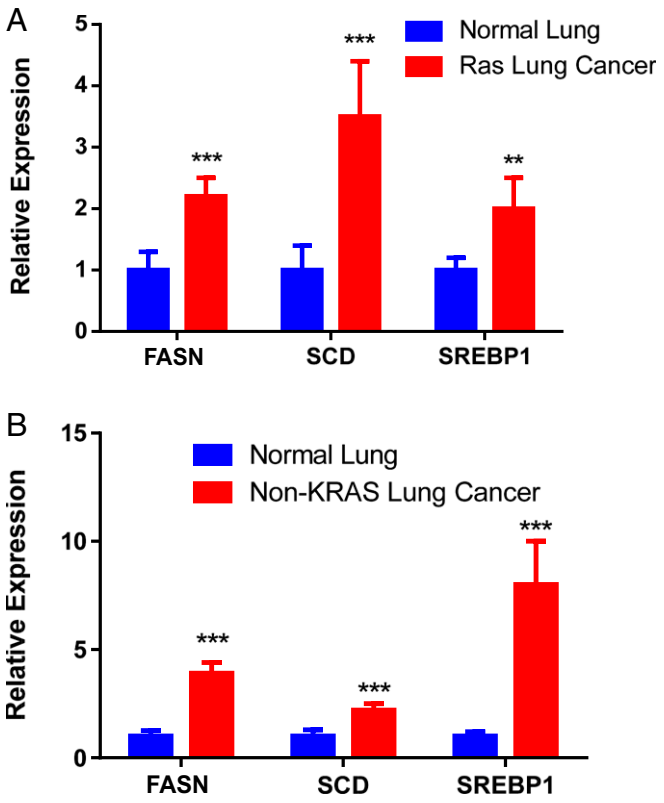

Fig. 2. Relative mRNA expression: (*A*) normal vs. human KRAS-associated lung cancer ($n = 12$) and (*B*) normal vs. human non-KRAS lung cancer ($n = 14$). **Statistical significance by *t* test for *P* value <0.01. ***Statistical significance by *t* test for *P* value <0.001.

where most complex glycerophospholipids are observed, an increase in the relative and total abundances of *m/z* 745.5034, glycerophosphoglycerol (PG; 18:1/16:1); *m/z* 747.5190, PG(18:1/16:0); *m/z* 793.5023, PG(18:2/20:4); and *m/z* 865.5034, PG(22:6/22:6) was detected. Changes in the relative and total abundances of free FAs in the *m/z* 200–400 were also observed, including *m/z* 255.2339, palmitic acid FA(16:0); *m/z* 281.2490, oleic acid FA (18:1); *m/z* 303.2333, arachidonic acid FA(20:4); and *m/z* 327.2334, docosahexaenoic acid, FA(22:6). All identifications were made by tandem MS (Table S2). Although the majority of these lipid species are common in both the adjacent normal tissues and normal lung control tissues, the total and relative abundances of these species are remarkably lower in normal tissue than in the cancer tissues. These results were consistently observed in other samples of KRAS-induced lung cancer and normal lung samples from other mice. Our results suggest that KRAS induces overexpression of lipids, including FAs and phospholipids, and is associated with a lipid profile that is distinct from normal lung tissues.

KRAS-Associated Induction of FASN Is Required for Lung Cancer Cell Proliferation. The human lung adenocarcinoma-associated cell lines A549 and H1299 cells are KRAS-positive (7, 31–33). Because we previously showed that KRAS activates ERK and FA synthesis genes, we administered the ERK inhibitor SCH772984 to both cell lines and found suppression of FASN and SCD (Fig. 5*A*). Moreover, KRAS inhibition (29) using *S*-trans,trans-farnesylthiosalicylic acid (FTS) decreased the gene expression of FASN and SCD in a dose-dependent manner as measured by qPCR (Fig. 5*B*). Therefore, KRAS inhibition impedes expression of lipogenesis-associated genes. To inhibit FA synthesis, we chose to inhibit FASN (Fig. S4) for several reasons. First, inhibition of SREBP would lead to suppression of various lipogenic pathways, not only the FA synthesis pathway (27). Second, inhibition of SCD would reduce the synthesis of only desaturated FAs but not saturated ones (25, 34). Third, FASN inhibition would be specific to the FA synthesis pathway, which would deplete both desaturated and saturated FA production (35, 36).

Cerulenin is an inhibitor of FASN (36, 37) (Fig. S4). Cerulenin treatment of mutated KRAS human lung adenocarcinoma cell lines A549 and H1299 resulted in decreased proliferation as measured by propidium iodide assay and hematocytometer (Fig. 6). Thus, the inhibition of FASN may present a potential treatment for KRAS-associated lung tumors.

Discussion

We found that we can distinguish between KRAS-positive and -negative lung adenocarcinoma as well as between neoplastic and normal lung tissue through (*i*) gene expression of FASN measured by qPCR, (*ii*) presence of ERK1 phosphoisoforms identified

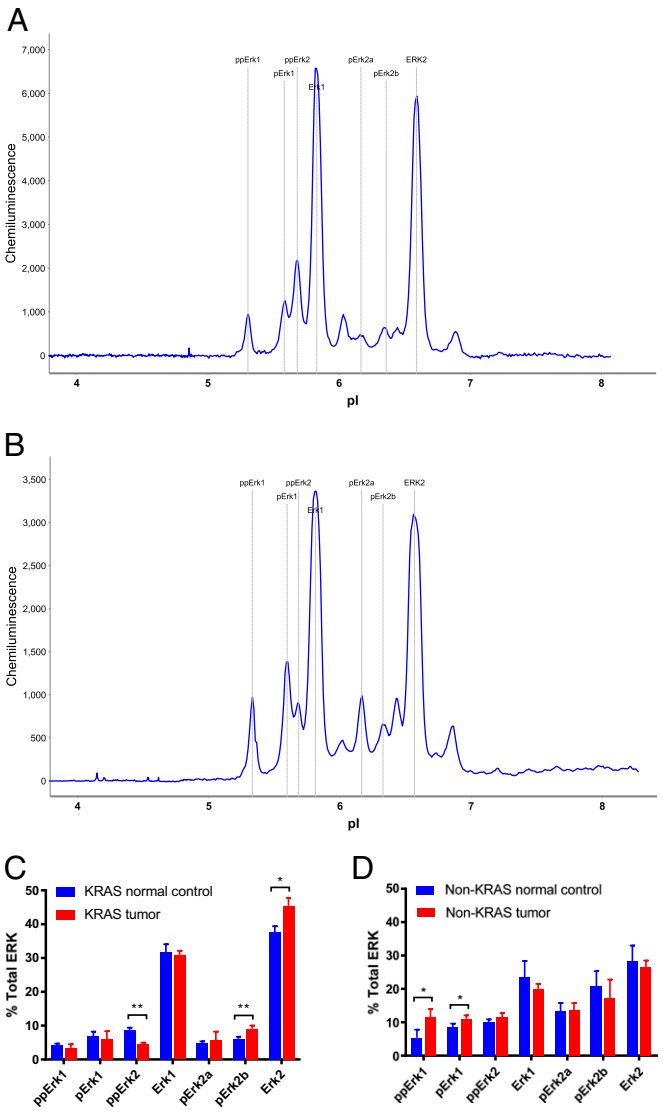

Fig. 3. NIA ERK protein signatures: (*A*) normal vs. human KRAS-associated lung cancer tissue ($n = 6$), (*B*) normal vs. human non-KRAS lung cancer tissue ($n = 6$), and percentages of total ERK in (*C*) KRAS tumors and (*D*) non-KRAS tumors. *Statistical significance by *t* test for *P* value <0.05. **Statistical significance by *t* test for *P* value <0.01.

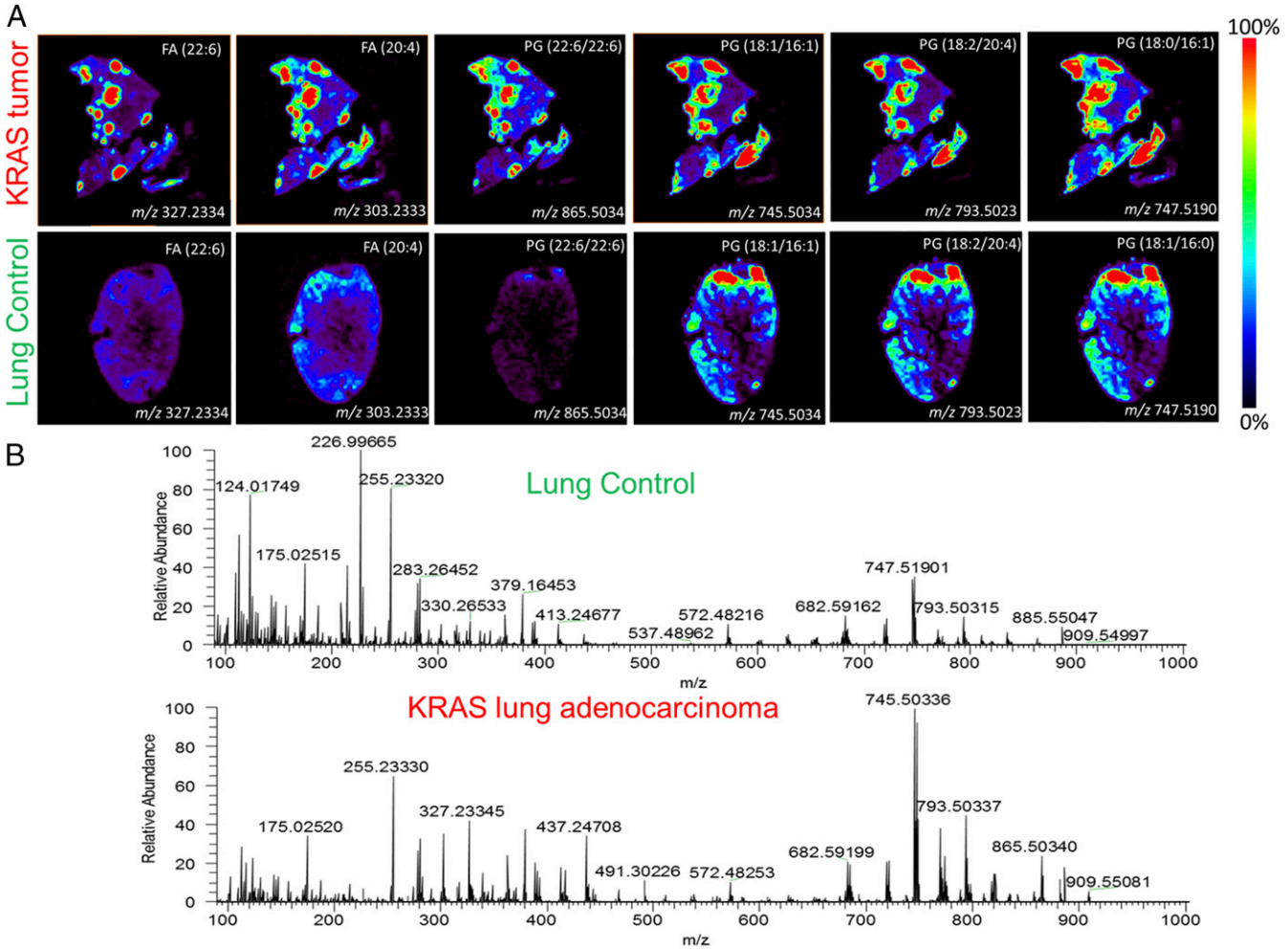

Fig. 4. DESI mass spectra of lipids: images of several lipid species overexpressed in (*Upper*) mouse tumor foci compared with normal mouse lung tissue and (*Lower*) corresponding representative mass spectra.

by the NIA, and (*iii*) the induction of unique lipid signature detected by DESI-MSI. The inhibition of KRAS with FTS blocked FASN expression and resulted in decreased lipogenesis. Moreover, the inhibition of FASN by cerulenin suppressed the proliferation of human KRAS-positive lung cancer cells. Hence, we have identified unique gene expression as well as proteomic and lipid signature for KRAS-positive lung adenocarcinoma.

Previous works showed that RAS family members can regulate glucose and glutamine metabolism (4–6). Based on this work, we suggest that KRAS gene causally controls lipogenesis. KRAS signaling is well-known to generally activate the ERK and MAPK pathways (29, 30). Our results show that this signaling induces lipogenesis through the induction of FASN and that it is mediated by ERK. Previous observations suggested that human tumors exhibit changes in lipid metabolism (36, 38). One possible mechanistic basis of this is through KRAS and ERK activation. However, lipogenesis in cancer in general is likely regulated through multiple mechanisms (27, 39).

We identified unique proteomic and lipid signatures of KRAS lung adenocarcinoma. By NIA, ERK1 vs. ERK2 protein activation allowed us to distinguish between KRAS-positive and -negative tumors in clinical specimens. NIA is a highly sensitive nanofluidic approach that is highly tractable for the examination of even picograms of protein derived from as few as 20 cells to measure proteins and their phosphorylation state (40, 41). Thus, NIA measurement of ERK may be useful in the diagnosis of lung adenocarcinoma.

Similarly, we identified a distinct lipid signature associated with KRAS-positive tumors by DESI-MSI. The unprecedented ability of this technique to examine metabolic changes in situ suggests that DESI-MSI can be used to distinguish between neoplastic and normal lung tissue, identify distinct genetic subtypes of lung cancer, and detect metabolomic alterations in lung tumors.

To date, lung adenocarcinomas seem to be incurable, despite the addition of both immunotherapeutics and EGF receptor (EGFR)-targeted therapies to conventional chemotherapy (42–44). Our results suggest that KRAS-induced lung adenocarcinoma may be particularly susceptible to the targeted therapeutic inhibition of FASN. More clinical work is needed to verify this hypothesis.

Materials and Methods

DESI-MSI. DESI-MSI was used for generating 2D chemical maps of 16-μm-thick tissue sections to assess the lipid profiles of tissue. The lung samples were snap-frozen in liquid nitrogen and stored at −80 °C before processing. The frozen samples were cut into 16-μm sections at −21 °C using a cryomicrotome and thaw-mounted onto microscope slides. The slides were stored at −80 °C. Before analysis, the slides were dried under a vacuum in a desiccator for ∼20 min. A laboratory-built DESI-MSI source coupled to an LTQ-Orbitrap-XL Mass Spectrometer (Thermo Fisher Scientific) was used, and DESI-MSI was performed in the negative ion mode at *m/z* 90–1,000 with a spatial resolution of 200 μm (Fig. S1). The Orbitrap was used as the mass analyzer while set to 60,000 resolving power. Mouse tissue samples were imaged by this method using dimethylformamide and acetonitrile (1:1) as a solvent system at a flow rate of 0.5 μL/min. The N_2

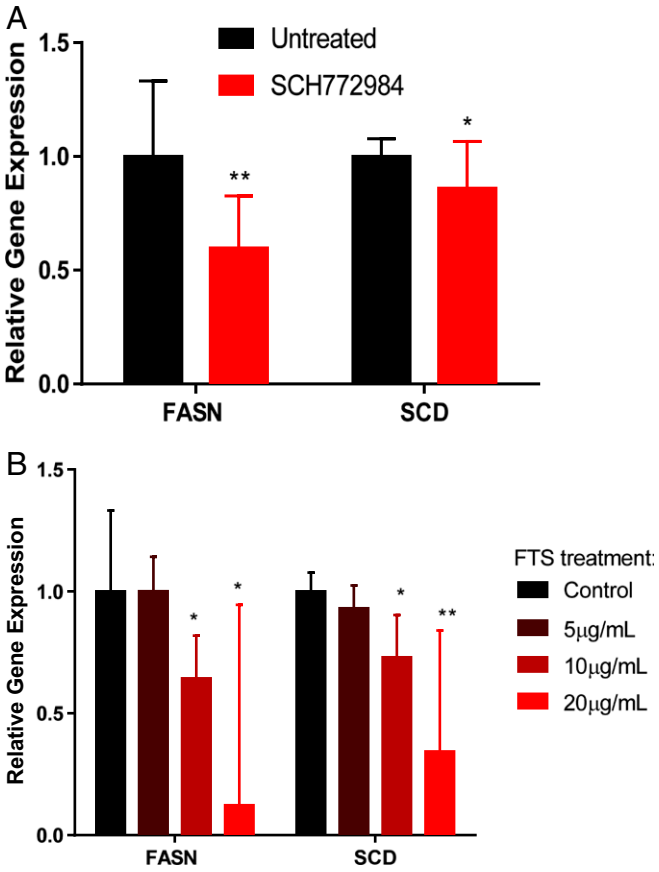

Fig. 5. Relative mRNA expression of FASN and SCD on (*A*) ERK inhibition by SCH772984 ($n = 3$) and (*B*) KRAS inhibition by FTS in the human lung cancer cell line ($n = 3$). Error bars represent 95% confidence intervals from Student's *t* distribution. *Statistical significance by unpaired two-sample *t* test for *P* value <0.05. **Statistical significance by unpaired two-sample *t* test for *P* value <0.01.

pressure was set to 175 psi. In DESI-MSI, charged solvents are sprayed onto the tissue, resulting in molecules, such as metabolites and lipids, being dissolved and extracted from the tissue surface and then transferred into a mass spectrometer for measurement of the *m/z* ratios. The software ImgGenerator (freeware; version 1.3) was used for converting raw files into 2D images. Spatially accurate ion images were assembled using BioMap software (freeware; ms-imaging.org/wp). After DESI-MSI, the same tissue section was subjected to a standard H&E staining for histopathologic evaluation using light microscopy. DESI-MS ion images were compared with optical microscopy images of the same tissue H&E-stained tissue sections for delineation of tumor foci. Tandem MS analyses were performed using both the Orbitrap and the linear ion trap for mass analysis to confirm lipid identity. The LipidMaps database (www.lipidmaps.org/) was also used to assist in lipid identification.

Patient Tissue Samples. Human lung adenocarcinoma samples with their matched normal tissue controls were purchased from the Vanderbilt University Thoracic Program Bio Repository, where informed consent was obtained from all participants under Institutional Review Board (IRB) Protocol 000616 approved by the Vanderbilt University Medical Center IRB Committee. The patient samples used in this study along with their KRAS mutations status are shown (Table S3).

Tetracycline-Based Conditional Murine Models. A Tet-On system was used to conditionally activate KRAS4b^{G12D}, an oncogenic form of a KRAS splice variant, in the lung tissue of transgenic mice. In this system, the gene encoding a reversible tetracycline transactivating factor (rtTA) is placed under the control of the Clara cell secretory protein (CCSP) promoter that drives its constitutive expression in lung Clara cells and type II pneumocytes. KRAS4b^{G12D} cDNA is placed under the control of the tetracycline-responsive minimal promoter (TetO-KRAS4b^{G12D}). In the absence of tetracycline, rtTA binds TetO sequences and represses transcription of the oncogene. In the presence of tetracycline, the binding of doxycycline to rtTA renders rtTA unable to bind TetO sequences, resulting in the activation of oncogene transcription. Mutant KRAS is activated by administering doxycycline (Sigma-Aldrich) to the drinking water (100 mg/mL) starting at the age of 4 wk. KRAS-induced lung tumors from four mice and normal lung tissues from three mice were harvested at week 24 and then analyzed by DESI-MSI. All animal studies were approved by the Stanford University Administrative Panel on Laboratory Animal Care. CCSP-rtTA/TetO-KRAS4b^{G12D} bitransgenic mice were used (23). An illustration of the Tet-On regulatory system present in these transgenic mice is shown (Fig. S2).

Microarray. Microarray analyses were performed by the Stanford Functional Genomics Facility using the Illumina WG6 mouse microarray platform. Whole-genome gene expression profiling was performed to compare gene expression for lung tissue from transgenic mice with KRAS turned on vs. KRAS turned off. The data were log2-transformed and quantile-normalized.

Cell Culture. The human nonsmall cell lung carcinoma cell lines, A549 and H1299, were used for in vitro experiments. A549 cells were maintained in DMEM supplemented with 10% (vol/vol) FBS, 1% L-glutamine, 1% sodium pyruvate, 1% nonessential amino acids, and Antibiotic–Antimycotic. H1299 cells were maintained in RPMI medium 1640 supplemented with 10% (vol/vol) FBS, 50 μM β-mercaptoethanol, and Antibiotic–Antimycotic. Trypsin-EDTA was used to passage both A549 and H1299 cells. All cell culture reagents were purchased from Gibco (Thermo Fisher Scientific Inc.).

Small Molecule Inhibitors. The small molecules, SCH772984 (Cayman) at 125 ng/mL, FTS (Sigma-Aldrich) at 5–20 ng/mL, and cerulenin (Sigma-Aldrich) at 1–10 μg/mL, were added to cell culture medium to achieve inhibition of ERK, KRAS, and FASN, respectively. FTS is a synthetic farnesylcysteine mimetic that interferes with the anchoring of KRAS to the plasma membrane (29). Cerulenin irreversibly inhibits FASN by covalently binding to the enzyme (36). Various levels of these drugs were administered to cells in culture over a time course to assess dose–response relationships.

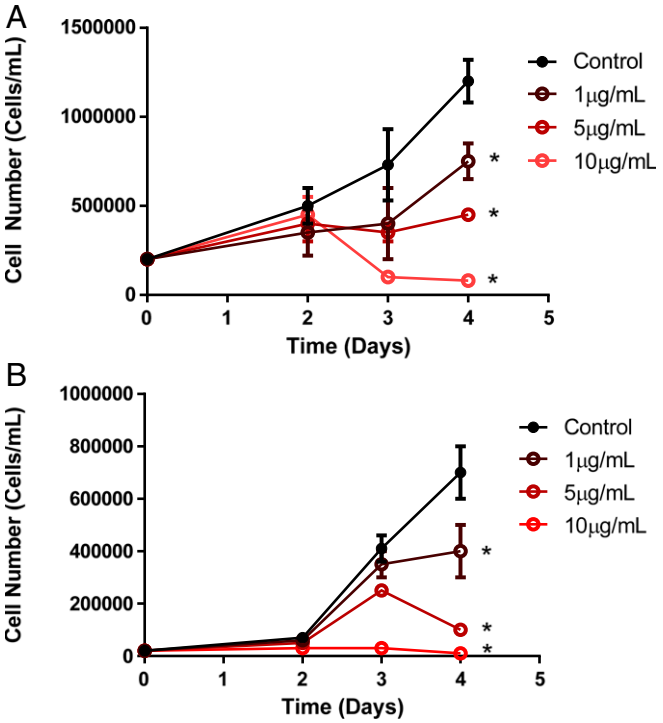

Fig. 6. Suppression of proliferation on inhibition of FASN by cerulenin in human lung cancer cell lines (*A*) A549 and (*B*) H1299 ($n = 3$ for each cell line). *Statistical significance by *t* test on day 4 compared with control for *P* value <0.05.

Cell Counting. A volume of cells was removed from culture medium and mixed with an equal volume of 0.4% Trypan blue stain. Then, 10 μL were taken out and placed into a hemocytometer for cell counting. Viable cell counts were used as a measure of cell proliferation.

RNA Extraction and cDNA Synthesis. Total RNA was isolated from cells and lung tissue using the QIAGEN RNeasy Mini Kit. RNA quality and concentration were assessed by the NanoDrop spectrophotometer. The RNA was reverse-transcribed into cDNA using the SuperScript III First-Strand Synthesis System (Invitrogen). All procedures were carried out according to the manufacturer's protocols.

Real-Time PCR. Real-time PCR was performed in 384-well plates on the QuantStudio 12K Flex Real-Time PCR System. Amplicons were detected by using SYBR Green I dye as fluorophore. Reactions were carried out in 20-μL volumes that contained 1 μL cDNA, 0.5 μM forward and reverse primers, and SYBR Green PCR Master Mix (Applied Biosystems). The amplification cycle was set as follows: 50 °C for 2 min; 95 °C for 10 min; and 40 cycles of 95 °C for 15 s, 60 °C for 1 min, and 72 °C for 30 s. After the amplification stage, a melt curve was performed to identify any nonspecific amplification. For each gene, a threshold cycle (Ct) number, which represents the number of cycles required to reach the threshold fluorescence, was determined. The Ct values were exported into Excel for statistical analysis. Ubiquitin was used as a housekeeping (reference) gene. The $2^{-\Delta\Delta CT}$ method was used to determine relative mRNA expression levels. Table S4 lists the real-time PCR primers used in this study.

NIA. NIA was performed using the Nanopro 1000 (Protein Simple) to detect the phosphorylation states of ERK1 and ERK2 in lysates generated from lung tumor tissue. NIA is a highly sensitive capillary-based isoelectric focusing method that uses antibody detection to quantify protein isoforms as well as characterize posttranslational protein modifications, such as phosphorylation. The final protein concentration loaded into each capillary of the Nanopro 1000 was 0.1 μg/μL. The primary rabbit antibody for ERK1/2 (Millipore) was diluted 1:300, and the primary mouse antibody for the loading control, Hsp70 (Santa Cruz Biosciences), was diluted 1:500. The anti-mouse and -rabbit secondary antibodies conjugated to HRP were diluted 1:100. Chemiluminescence signal was recorded after the addition of luminol and peroxide detection reagents. Analysis of NIA data was performed in Compass software (Protein Simple).

Statistical Analysis. Error bars were constructed based on calculated SD values. The error bars represent the means ± SDs. Where appropriate, a Student's *t* test was used to assess statistical significance. Statistical significance by *t* test is indicated by $*P$ value <0.05, $**P$ value <0.01, and $***P$ value <0.001.

ACKNOWLEDGMENTS. We thank Harold Varmus for the CCSP-rtTA/TetO-KRAS4b^{G12D} bitransgenic mice, and are grateful to Translational Applications Service Center at Stanford for the Nano Immuno Assay experiments. A.M.G. and K.M. acknowledge Stanford Cancer Translational Nanotechnology Training T32 Training Grant T32 CA196585 funded by the National Cancer Institute and the Stanford Center of Molecular Analysis and Design, respectively. This work is supported by NIH Grant R01CA184384.

1. Osada H, Takahashi T (2002) Genetic alterations of multiple tumor suppressors and oncogenes in the carcinogenesis and progression of lung cancer. *Oncogene* 21(48): 7421–7434.
2. Jancík S, Drábek J, Radzioch D, Hajdúch M (2010) Clinical relevance of KRAS in human cancers. *J Biomed Biotechnol* 2010:150960.
3. Karachaliou N, et al. (2013) KRAS mutations in lung cancer. *Clin Lung Cancer* 14(3): 205–214.
4. Gaglio D, et al. (2011) Oncogenic K-Ras decouples glucose and glutamine metabolism to support cancer cell growth. *Mol Syst Biol* 7:523.
5. Ying H, et al. (2012) Oncogenic Kras maintains pancreatic tumors through regulation of anabolic glucose metabolism. *Cell* 149(3):656–670.
6. Son J, et al. (2013) Glutamine supports pancreatic cancer growth through a KRAS-regulated metabolic pathway. *Nature* 496(7443):101–105.
7. Li J, Wang S, Su ZF, Yuan Y (2016) Synergistic effects of sorafenib in combination with gemcitabine or pemetrexed in lung cancer cell lines with K-ras mutations. *Contemp Oncol (Pozn)* 20(1):33–38.
8. Wise DR, Thompson CB (2010) Glutamine addiction: A new therapeutic target in cancer. *Trends Biochem Sci* 35(8):427–433.
9. Kriegsmann M, et al. (2016) Reliable entity subtyping in non-small cell lung cancer by matrix-assisted laser desorption/ionization imaging mass spectrometry on formalin-fixed paraffin-embedded tissue specimens. *Mol Cell Proteomics* 15(10):3081–3089.
10. Li T, et al. (2015) In situ biomarker discovery and label-free molecular histopathological diagnosis of lung cancer by ambient mass spectrometry imaging. *Sci Rep* 5: 14089.
11. Takáts Z, Wiseman JM, Gologan B, Cooks RG (2004) Mass spectrometry sampling under ambient conditions with desorption electrospray ionization. *Science* 306(5695): 471–473.
12. Wiseman JM, Ifa DR, Song Q, Cooks RG (2006) Tissue imaging at atmospheric pressure using desorption electrospray ionization (DESI) mass spectrometry. *Angew Chem Int Ed Engl* 45(43):7188–7192.
13. Amstalden van Hove ER, Smith DF, Heeren RM (2010) A concise review of mass spectrometry imaging. *J Chromatogr A* 1217(25):3946–3954.
14. Eberlin LS, et al. (2014) Alteration of the lipid profile in lymphomas induced by MYC overexpression. *Proc Natl Acad Sci USA* 111(29):10450–10455.
15. Shroff EH, et al. (2015) MYC oncogene overexpression drives renal cell carcinoma in a mouse model through glutamine metabolism. *Proc Natl Acad Sci USA* 112(21): 6539–6544.
16. Zhang J, et al. (2016) Cardiolipins are biomarkers of mitochondria-rich thyroid oncocytic tumors. *Cancer Res* 76(22):6588–6597.
17. Eberlin LS, et al. (2016) Pancreatic cancer surgical resection margins: Molecular assessment by mass spectrometry imaging. *PLoS Med* 13(8):e1002108.
18. Calligaris D, et al. (2014) Application of desorption electrospray ionization mass spectrometry imaging in breast cancer margin analysis. *Proc Natl Acad Sci USA* 111(42):15184–15189.
19. Jarmusch AK, et al. (2016) Lipid and metabolite profiles of human brain tumors by desorption electrospray ionization-MS. *Proc Natl Acad Sci USA* 113(6):1486–1491.
20. Tata A, et al. (2016) Rapid detection of necrosis in breast cancer with desorption electrospray ionization mass spectrometry. *Sci Rep* 6:35374.
21. Relat J, et al. (2012) Different fatty acid metabolism effects of (-)-epigallocatechin-3-gallate and C75 in adenocarcinoma lung cancer. *BMC Cancer* 12:280.
22. Orita H, et al. (2007) Selective inhibition of fatty acid synthase for lung cancer treatment. *Clin Cancer Res* 13(23):7139–7145.
23. Fisher GH, et al. (2001) Induction and apoptotic regression of lung adenocarcinomas by regulation of a K-Ras transgene in the presence and absence of tumor suppressor genes. *Genes Dev* 15(24):3249–3262.
24. Menendez JA, Lupu R (2007) Fatty acid synthase and the lipogenic phenotype in cancer pathogenesis. *Nat Rev Cancer* 7(10):763–777.
25. Dobrzyn P, et al. (2004) Stearoyl-CoA desaturase 1 deficiency increases fatty acid oxidation by activating AMP-activated protein kinase in liver. *Proc Natl Acad Sci USA* 101(17):6409–6414.
26. Yang F, et al. (2006) An ARC/Mediator subunit required for SREBP control of cholesterol and lipid homeostasis. *Nature* 442(7103):700–704.
27. Lewis CA, et al. (2015) SREBP maintains lipid biosynthesis and viability of cancer cells under lipid- and oxygen-deprived conditions and defines a gene signature associated with poor survival in glioblastoma multiforme. *Oncogene* 34(40):5128–5140.
28. Almeida L, Lochner M, Berod L, Sparwasser T (2016) Metabolic pathways in T cell activation and lineage differentiation. *Semin Immunol* 28(5):514–524.
29. Tsujino I, et al. (2016) Increased phosphorylation of ERK1/2 is associated with worse chemotherapeutic outcome and a poor prognosis in advanced lung adenocarcinoma. *Med Mol Morphol* 49(2):98–109.
30. Yamakawa K, et al. (2016) Activation of MEK1/2-ERK1/2 signaling during NNK-induced lung carcinogenesis in female A/J mice. *Cancer Med* 5(5):903–913.
31. Kharbanda A, et al. (2014) MUC1-C confers EMT and KRAS independence in mutant KRAS lung cancer cells. *Oncotarget* 5(19):8893–8905.
32. Shindo-Okada N, Takeuchi K, Han BS, Nagamachi Y (2002) Establishment of cell lines with high and low metastatic potential from A549 human lung adenocarcinoma. *Jpn J Cancer Res* 93(1):50–60.
33. Amaar YG, et al. (2006) Ras association domain family 1C protein stimulates human lung cancer cell proliferation. *Am J Physiol Lung Cell Mol Physiol* 291(6):L1185–L1190.
34. Young RM, et al. (2013) Dysregulated mTORC1 renders cells critically dependent on desaturated lipids for survival under tumor-like stress. *Genes Dev* 27(10):1115–1131.
35. Yilmaz A, et al. (2014) Increased NQO1 but not c-MET and survivin expression in non-small cell lung carcinoma with KRAS mutations. *Int J Environ Res Public Health* 11(9): 9491–9502.
36. Kuhajda FP, et al. (2000) Synthesis and antitumor activity of an inhibitor of fatty acid synthase. *Proc Natl Acad Sci USA* 97(7):3450–3454.
37. Flavin R, Peluso S, Nguyen PL, Loda M (2010) Fatty acid synthase as a potential therapeutic target in cancer. *Future Oncol* 6(4):551–562.
38. Dang CV (2013) MYC, metabolism, cell growth, and tumorigenesis. *Cold Spring Harb Perspect Med* 3(8):a014217.
39. Carroll PA, et al. (2015) Deregulated Myc requires MondoA/Mlx for metabolic reprogramming and tumorigenesis. *Cancer Cell* 27(2):271–285.
40. Fan AC, et al. (2009) Nanofluidic proteomic assay for serial analysis of oncoprotein activation in clinical specimens. *Nat Med* 15(5):566–571.
41. Fan AC, O'Rourke JJ, Praharaj DR, Felsher DW (2013) Real-time nanoscale proteomic analysis of the novel multi-kinase pathway inhibitor rigosertib to measure the response to treatment of cancer. *Expert Opin Investig Drugs* 22(11):1495–1509.
42. Naidoo J, Drilon A (2016) KRAS-mutant lung cancers in the era of targeted therapy. *Adv Exp Med Biol* 893:155–178.
43. Ahsan A (2016) Mechanisms of resistance to EGFR tyrosine kinase inhibitors and therapeutic approaches: An update. *Adv Exp Med Biol* 893:137–153.
44. Umelo IA, et al. (2015) Combined targeting of EGFR/HER promotes anti-tumor efficacy in subsets of KRAS mutant lung cancer resistant to single EGFR blockade. *Oncotarget* 6(24):20132–20144.